

COSMOLOGICAL CONSTRAINTS FROM THE REDSHIFT DEPENDENCE OF THE ALCOCK-PACZYNSKI EFFECT: FOURIER SPACE ANALYSIS

XIAOLIN LUO, ZIYONG WU, XIAO-DONG LI, MIAO LI,
School of Physics and Astronomy, Sun Yat-Sen University, Guangzhou 510297, P.R.China

ZHIGANG LI
Nanyang Normal University, 1638 Wolong Rd, Wolong, Nanyang, China

CRISTIANO G. SABIU
Department of Astronomy, Yonsei University, 50 Yonsei-ro, Seodaemun-gu, Seoul, 03722, Korea
Draft version March 26, 2022

ABSTRACT

The tomographic Alcock-Paczynski (AP) method utilizes the redshift evolution of the AP distortion to place constraints on cosmological parameters. It has proved to be a robust method that can separate the AP signature from the redshift space distortion (RSD) effect, and deliver powerful cosmological constraints using the $\lesssim 40h^{-1}$ Mpc clustering region. In previous works, the tomographic AP method was performed via the anisotropic 2-point correlation function statistic. In this work we consider the feasibility of conducting the analysis in the Fourier domain and examine the pros and cons of this approach. We use the integrated galaxy power spectrum (PS) as a function of direction, $\hat{P}_{\Delta k}(\mu)$, to quantify the magnitude of anisotropy in the large-scale structure clustering, and use its redshift variation to do the AP test. The method is tested on the large, high resolution Big-MultiDark Planck (BigMD) simulation at redshifts $z=0-1$, using the underlying true cosmology $\Omega_m=0.3071$, $w=-1$. Testing the redshift evolution of $\hat{P}_{\Delta k}(\mu)$ in the true cosmology and cosmologies deviating from the truth with $\delta\Omega_m=0.1$, $\delta w=0.3$, we find that the redshift evolution of the AP distortion overwhelms the effects created by the RSD by a factor of $\sim 1.7-3.6$. We test the method in the range of $k \in (0.2, 1.8) h \text{ Mpc}^{-1}$, and find that it works well throughout the entire regime. We tune the halo mass within the range 2×10^{13} to $10^{14} M_\odot$, and find that the change of halo bias results in $\lesssim 5\%$ change in $\hat{P}_{\Delta k}(\mu)$, which is less significant compared with the cosmological effect. Our work shows that it is feasible to conduct the tomographic AP analysis in the Fourier space.

Subject headings: large-scale structure of Universe — dark energy — cosmological parameters

1. INTRODUCTION

The large-scale structure (LSS) of the Universe contains enormous information about the expansion and structure growth histories of our Universe. In the past two decades, large-scale surveys of galaxies has greatly enriched our understanding about the Universe (York et al. 2000; Colless et al. 2003; Eisenstein et al. 2005; Percival et al. 2007; Blake et al. 2011b,a; Beutler et al. 2012; Anderson et al. 2012; Alam et al. 2017), while the future surveys will enable us to measure the $z \lesssim 1.5$ Universe in unprecedented precision, shedding light on the dark energy problem (Riess et al. 1998; Perlmutter et al. 1999; Weinberg 1989; Li et al. 2011; Weinberg et al. 2013).

The well-known Alcock-Paczynski (AP) test (Alcock & Paczynski 1979) is a geometric method for probing the cosmic expansion history using the LSS. Under a certain cosmological model, the radial and tangential sizes of distant objects or structures take the forms of $\Delta r_{\parallel} = \frac{c}{H(z)} \Delta z$ and $\Delta r_{\perp} = (1+z)D_A(z)\Delta\theta$, where Δz , $\Delta\theta$ are their redshift span and angular size, while D_A , H being the angular diameter distance and the Hubble parameter, respectively.

Assuming incorrect models for computing D_A and H results in miss-estimated values of Δr_{\parallel} and Δr_{\perp} , which manifest themselves as geometric distortions along the line-of-sight (LOS) and perpendicular directions. This distortion, known

as the AP distortion, can be measured and quantified via statistical analysis of the large-scale galaxy distribution, and thus is widely used in LSS survey analyses to constrain the cosmological parameters (Ryden 1995; Ballinger et al. 1996; Matsubara & Suto 1996; Outram et al. 2004; Blake et al. 2011b; Lavaux & Wandelt 2012; Alam et al. 2017; Mao et al. 2017; Ramanah et al. 2019).

The “tomographic AP method” is a novel technique of applying the AP test to the LSS (Li et al. 2014, 2015; Park et al. 2019), which has achieved tight constraints on the parameters governing the cosmic expansion. The concept of the method is to utilize the *redshift evolution* of the LSS anisotropy, which is sensitive to the AP effect, while being insensitive to the distortion produced by the redshift space distortions (RSD). This makes it possible to differentiate the AP distortion from the large contamination of RSD. Li et al. (2015) proposed to quantify the anisotropic clustering via $\hat{\xi}_{\Delta s}(\mu)$, which is defined as an integration of the 2D $\xi(s, \mu)$ over the clustering scale s . Li et al. (2016) firstly applied the method to the SDSS (Sloan Digital Sky Survey) BOSS (Baryon Oscillation Spectroscopic Survey) DR12 galaxies, and achieved $\sim 35\%$ improvements in the constraints on the ratio of dark matter Ω_m and dark energy equation of state (EOS) w . In later works, Li et al. (2018); Zhang et al. (2019) found the method greatly improves the constraints on dynamical dark energy models, while the analysis of Li et al. (2019) showed that, in the case

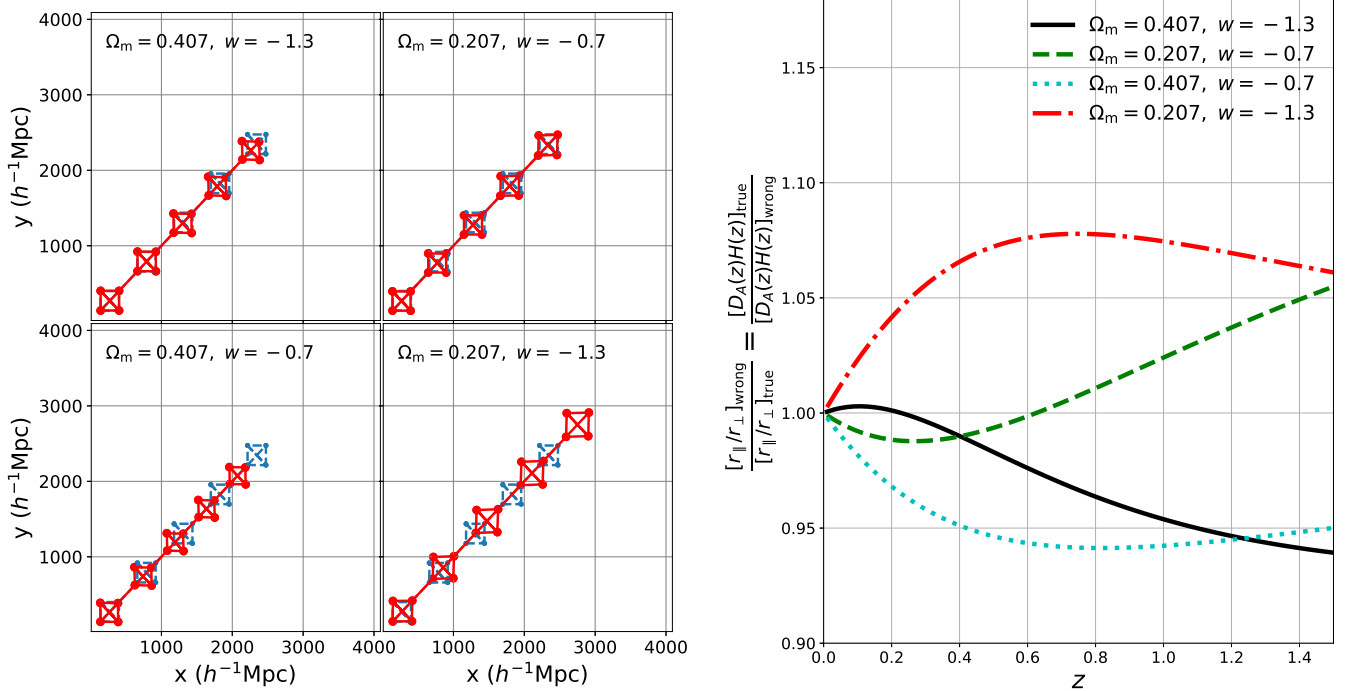


FIG. 1.— Examples of shapes distorted due to the AP effect, in the case of adopting four incorrect sets of cosmologies in a fiducial cosmology of $\Omega_m = 0.307$, $w = -1$. In the left panel, we plot the underlying true shapes of the 5 perfect squares with blue dashed lines, while their distorted shapes in the wrong cosmologies are showed by red solid lines. The observer was placed at the origin of the 2D coordinates. In the right panel we plot the magnitude of the shape distortions as a function of redshift (Equation 4).

of using DESI-like data¹, combining the method with the CMB+BAO datasets can improve the dark energy figure-of-merit (Wang 2008) by a factor of 10.

In this work, we extend the scope of the previous studies and investigate how to conduct the tomographic AP test using the power spectrum (PS). The PS is the Fourier transform of the two-point correlation function. Compared to the correlation function in configuration space, the PS has advantages such as milder coupling among the different k -modes, it is more closely related to theoretical models, and so on. Thus it has been widely adopted as a standard tool in galaxy clustering analysis. It is worthwhile developing a methodology to conduct the tomographic AP method in the Fourier space, and the result will serve as a cross-check to the configuration space result.

The rest of this paper is organized as follows. In Sec.2, we briefly introduce the physics of the AP test as well as our methodology. In Sec.3, we describe the N-body simulation and the halo samples used in this work. We present the results in Sec.4, and conclude in Sec.5.

2. METHODOLOGY

2.1. The Alcock-Paczynski Test in a Nutshell

The so called AP effect (Alcock & Paczynski 1979) refers to the apparent geometric distortions in the LSS that arise when incorrect cosmological models are assumed for transforming the observed galaxy redshifts into comoving distances. For a distant object or structure in the Universe, one can calculate its size along and across the LOS using the formulas of

$$r_{\parallel} = \frac{c}{H(z)} \Delta z, \quad r_{\perp} = (1+z)D_A(z)\Delta\theta. \quad (1)$$

¹ <https://desi.lbl.gov/>

Here Δz and $\Delta\theta$ are the observed redshift span and angular size measured via observations, while H and D_A are the Hubble parameter and the angular diameter distance, respectively. In a spatially flat Universe composed of a dark matter component with current ratio Ω_m and a dark energy component with constant EOS w , they take the forms of

$$H(z) = H_0 \sqrt{\Omega_m a^{-3} + (1 - \Omega_m) a^{-3(1+w)}}, \quad (2)$$

$$D_A(z) = \frac{1}{1+z} r(z) = \frac{1}{1+z} \int_0^z \frac{cdz'}{H(z')}, \quad (3)$$

where $a = 1/(1+z)$ is the cosmic scale factor, H_0 is the current Hubble parameter and $r(z)$ is the comoving distance.

Adopting a wrong set of Ω_m and w results in miss-estimated values of r_{\parallel} and r_{\perp} . Consequently, the constructed objects have distorted shapes (AP effect) and incorrect volume elements (volume effect), whose magnitudes are

$$\frac{\text{Shape}_{\text{wrong}}}{\text{Shape}_{\text{true}}} = \frac{[r_{\parallel}/r_{\perp}]_{\text{wrong}}}{[r_{\parallel}/r_{\perp}]_{\text{true}}} = \frac{[D_A(z)H(z)]_{\text{true}}}{[D_A(z)H(z)]_{\text{wrong}}}, \quad (4)$$

$$\frac{\text{Volume}_{\text{wrong}}}{\text{Volume}_{\text{true}}} = \frac{[(r_{\parallel}r_{\perp})^2]_{\text{wrong}}}{[(r_{\parallel}r_{\perp})^2]_{\text{true}}} = \frac{[(D_A(z))^2/H(z)]_{\text{wrong}}}{[(D_A(z))^2/H(z)]_{\text{true}}}. \quad (5)$$

In galaxy surveys, measuring the galaxy clustering in the radial and transverse directions leads to measurements of $D_A(z)$ and $H(z)$, which enables us to place constraints on the cosmological parameters therein.

In Figure 1 we illustrate the AP distortions for four incorrect cosmologies. The figure shows that, not only the shapes of the distributions are distorted, but also a redshift dependence in the distortion appears in each cosmology. Based on this fact, Li et al. (2014, 2015) proposed the tomographic AP

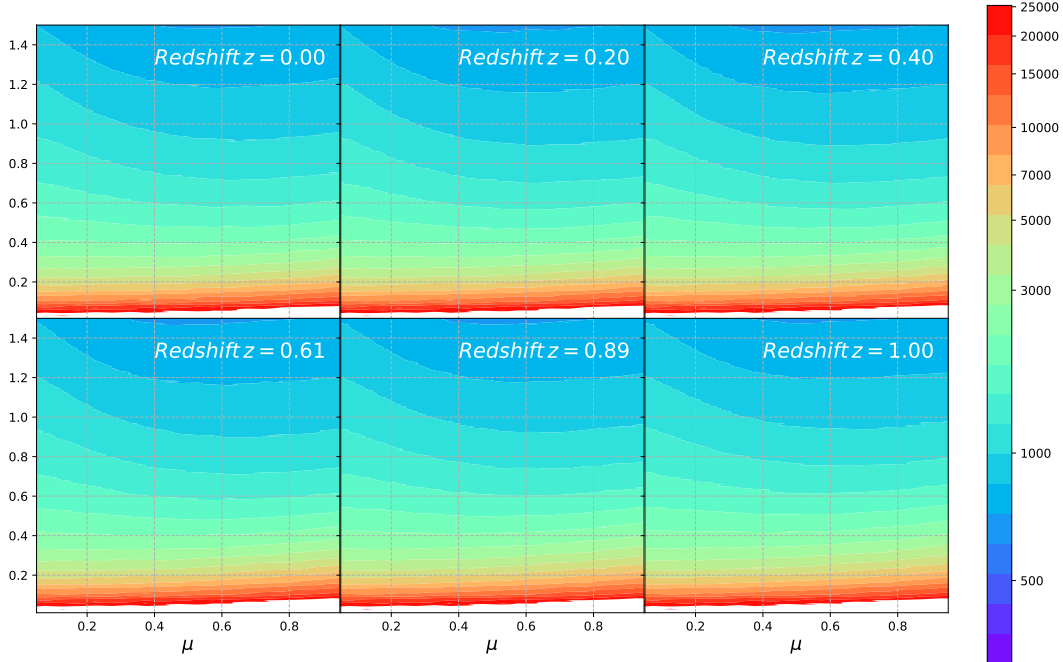


FIG. 2.— The 2D PS $P(k, \mu)$ of the BigMD halos measured at 6 redshifts distributed in $z \in [0, 1]$, in the framework of the true cosmology (the simulation cosmology). The RSD effect produces anisotropies in the halo distribution, and manifests itself as the non-horizontal contour lines. The similarity among the 6 panels shows that in different redshifts the anisotropy created by the RSD maintains a similar pattern.

method, which probes the AP distortion by measuring the redshift evolution of the anisotropic galaxy clustering.

2.2. Tomographic AP test using PS

Li et al. (2014) proposed a tomographic analysis of the small scale galaxy clustering to efficiently separate the AP effect from the RSD. They used the integrated correlation function at various LOS directions, $\hat{\xi}_{\Delta_s}(\mu)$, to quantify the magnitude of anisotropy at different redshifts. Li et al. (2015) applied the method to the SDSS galaxy samples and obtained tight cosmological constraints. It is worthy to develop a similar method in Fourier space, as an alternative way to conduct the tomographic AP analysis.

Using the PS statistics has many advantages over using the correlation function in configuration space, such as,

- In the PS, clustering signals at different scales are uncorrelated, while in configuration space there exists strong mode-coupling. By using the PS analysis we can more easily prohibit the clustering signal in the heavily non-linear region from entering a wide range of modes and causing arduous complexity. Also, being more clear about what physical scales are used in the analysis, we can have a better understanding about the method.
- Compared with the configuration space, in Fourier space it is more convenient to calculate the theoretical predictions of the statistical quantities.
- The computation of the PS can be much faster than the 2-point correlation function.

In this work, we adopt the open-source tool `Nbodykit` (Hand et al. 2018) to calculate the 2D PS. The redshift-space data is assigned to a discrete mesh using the `to_mesh` function with the default Cloud-In-Cell window, and the values

of $P(k, \mu)$ are then computed using the Fast Fourier Transform (Bianchi et al. 2015; Scoccimarro 2015). Here k is the wavenumber, and μ represents the cosine of the angle between line of sight and wavenumber.

In conducting the AP test we first measure the 2D PS $P(k, \mu)$ of the BigMD sample. Following the concept of Li et al. (2015), we then integrate $P(k, \mu)$ over the wavenumber k , to build up a statistical quantity that solely depends on the direction μ ,

$$P_{\Delta k}(\mu) \equiv \int_{k_{\min}}^{k_{\max}} P(k, \mu) dk. \quad (6)$$

To reduce the effect of the clustering strength and galaxy bias, we further conduct a normalization, which is expressed as

$$\hat{P}_{\Delta k}(\mu) \equiv \frac{P_{\Delta k}(\mu)}{\int_0^1 P_{\Delta k}(\mu) d\mu}. \quad (7)$$

Li et al. (2015, 2016) suggested using $s = 6 - 40h^{-1}\text{Mpc}$ for $\hat{\xi}_{\Delta_s}(k, \mu)$. This corresponds to a k range of $\sim (0.15 - 1) h \text{ Mpc}^{-1}$. In this work, we will test several choices of (k_{\min}, k_{\max}) , to gain some understanding about which range of k is most optimal for this analysis.

3. MOCK

For the testing of the new method we use the Big-MultiDark Planck (BigMD) simulation (Klypin et al. 2016), whose size and resolution is close to the Horizon Run N-body simulations (Kim et al. 2009, 2015) used in Li et al. (2014, 2015, 2016). The simulation was produced using 3840^3 particles in a volume of $(2.5h^{-1}\text{Gpc})^3$, assuming a ΛCDM cosmology with parameters $\Omega_m = 0.307115$, $\Omega_b = 0.048206$, $\sigma_8 = 0.8288$, $n_s = 0.9611$, and $H_0 = 67.77\text{km s}^{-1}\text{Mpc}^{-1}$. This yields a mass resolution of $2.4 \times 10^{10}h^{-1}M_{\odot}$. The initial condition was set by using the Zeldovich approximation at redshift $z_{\text{init}} = 100$.

From the simulation particles, halo catalogues at 78 snapshots are generated using the Rockstar algorithm (Behroozi et al. 2013). The large volume, high resolution resolution and wide redshift coverage of the simulation makes it among the best choices for testing our methodology.

The snapshots chosen for the Fourier space analysis of AP effect have redshifts of 0, 0.2, 0.4, 0.61, 0.89 and 1.0, respectively. By applying different minimal mass cuts at different redshifts to maintain a constant number density $\bar{n} = 10^{-3} (h^{-1}\text{Mpc})^{-3}$ in all snapshots. This number density is close to the galaxy number density of current and next generation spectroscopic galaxy surveys. To mimick the redshift-space distortions (RSD) caused by galaxy peculiar velocities, we perturb the positions of halos along the z -direction, using the following formula

$$\Delta z = (1+z) \frac{v_{\text{LOS}}}{c}, \quad (8)$$

where v_{LOS} is the line-of-sight (LOS) component of the peculiar velocity of halos.

4. RESULTS

In this work, we compute the 2D PS of the mock data, using different snapshots and also different assumptions of cosmologies.

4.1. The 2D PS at different redshifts

Figure 2 shows the 2D contour map of the power spectra $P(k, \mu)$ at six redshifts. The regions $k \in (0.2, 1.0) h \text{ Mpc}^{-1}$ are marked by the two dashed lines.

In the $k \lesssim 0.2$ regions the pattern of $P(k, \mu)$ behaves as its linear behavior $P \propto (1 + \beta\mu^2)^2$ (Kaiser 1987), where $\beta \equiv bf$ and b, f is the bias and the growth rate, respectively. This relation completely breaks down at $k \gtrsim 0.5$, where we see the PS maximizes at $\mu \sim 0$, reaches its minimal value at $\mu \approx 0.6$, and possesses another peak-value at $\mu \sim 1$.

From the plot we find the PS measured at the six redshifts look rather close to each other. Even though it is difficult to precisely model the $P(k, \mu)$ in the non-linear region still we can make use of this redshift ‘‘invariance’’ to conduct a cosmological analysis.

4.2. $\hat{P}_{\Delta k}(\mu)$ in the True Cosmology

The integrated PS $\hat{P}_{\Delta k}(\mu)$ are plotted in Figure 3, where we show the results in the fiducial cosmology of the BigMD simulation as well as a wrong cosmology $\Omega_m = 0.407, w = -1.30$. From left to right, we use integration intervals of (0.2, 0.4), (0.4, 0.6), (0.6, 0.8) and (0.8, 1.0) $h \text{ Mpc}^{-1}$, respectively. We find that:

- In the first panel ($k \in (0.2, 0.4) h \text{ Mpc}^{-1}$), the curves only have a rising trend along μ , suggesting that their behaviours are dominated by the Kaiser effect Kaiser (1987).
- In the second panel ($k \in (0.4, 0.6) h \text{ Mpc}^{-1}$), the curves decline at $\mu \lesssim 0.55$. This phenomenon is caused by the FOG effect. On smaller scales, the FOG effects will dominate the linear Kaiser effects over almost all μ values. However, at large μ values (> 0.5) the higher-order nonlinear terms play an important role and can even force the curves to turn over (see (Zheng & Song 2016) for details).

- In the last two panels ($k \in (0.6, 0.8), (0.8, 1.0) h \text{ Mpc}^{-1}$), as k becomes larger, the impact of the FOG effect becomes stronger. This makes the declining trend in $\mu \lesssim 0.6$ stronger, and the rising trend in $0.6 < \mu < 1.0$ weaker.

In Figure 4 we plotted the redshift evolution of $\hat{P}_{\Delta k}(\mu)$, quantified as

$$\delta \hat{P}_{\Delta k}(\mu, z_1, z_2) \equiv \hat{P}_{\Delta k}(\mu, z_1) - \hat{P}_{\Delta k}(\mu, z_2) \quad (9)$$

where we choose $z_0 = 0$ and $z_i = 0, 0.2, 0.4, 0.61, 0.89, 1$. Results of the true Cosmology (upper panel) show weak and non-zero redshift evolutions in all range of k . The evolutions become smaller as we increase the values of k .

4.3. $\hat{P}_{\Delta k}(\mu)$ and its Redshift Evolution in the Wrong Cosmology

In the lower panels Figure 3 and 4 we plot $\hat{P}_{\Delta k}(\mu)$ and its redshift evolution in a wrong cosmology $\Omega_m = 0.407, w = -1.30$. Figure 1 shows that that, at $z < 0.2$ ($z > 0.2$), this cosmology creates compression (stretch) along the LOS, and the magnitude of compression/stretch largely depends on the redshift.

Correspondingly, in the lower panel of Figure 3, we see an extra tilt in the PS – compared with the true cosmology results, in the wrong cosmology the $\hat{P}_{\Delta k}(\mu)$ s have smaller (larger) values in the region of $\mu \lesssim 0.5$ ($\mu \gtrsim 0.5$). The redshift evolution of the anisotropy manifests itself as a redshift evolution of $\hat{P}_{\Delta k}(\mu)$. In the lower panel Figure 4, we find that the wrong cosmology yields larger $\hat{P}_{\Delta k}(\mu, z_i) - \hat{P}_{\Delta k}(\mu, z_0)$ than the true cosmology results at $z > 0.2$.

Using different integration range of k , the additional evolution created by AP is also different. To have a understanding about their values, we list the value of $\delta \hat{P}_{\Delta k}(\mu = 1, z_1 = 0, z_2 = 1)$ in Table 1, which clearly shows that the wrong cosmology yields to larger values of $\delta \hat{P}_{\Delta k}$. Using different choices of $(k_{\text{min}}, k_{\text{max}})$, we find

$$\frac{\delta \hat{P}_{\Delta k, \text{wrong cosmology}}}{\delta \hat{P}_{\Delta k, \text{true cosmology}}} \approx 1.7 - 3.6. \quad (10)$$

4.4. More Tests on the Integration Range and Cosmologies

To test the method in wider clustering range we perform a test using k up to $1.8 h \text{ Mpc}^{-1}$ Figure 5 shows the results in case that we use the integration range of $k \in (0.2, 0.6), (0.6, 1), (1, 1.4)$ and $(1.4, 1.8) h \text{ Mpc}^{-1}$. The values of $\Delta \hat{P}_{\Delta k}(\mu)$ and $\delta \Delta \hat{P}_{\Delta k}(\mu)$ decreases as we increase the value of k . In all cases, the wrong cosmology leads to larger redshift evolution than the true cosmology. So in optimistic case we may be able to use the non-linear regime of $k = 1.8 h \text{ Mpc}^{-1}$.

To test it in more cosmologies, in Figure 6 we further plot $\delta \hat{P}_{\Delta k}(\mu)$ in four cosmologies of $(\Omega_m, w) = (0.307, -1), (0.407, -1), (0.307, -0.7)$ and $(0.407, -0.7)$. We find larger $\delta \hat{P}_{\Delta k}$ in all wrong cosmologies. This suggests that the enlarged redshift evolution of $\hat{P}_{\Delta k}$ is a universal phenomenon which can be found in a large space of wrong parameters.

4.5. A Test about Halo Bias

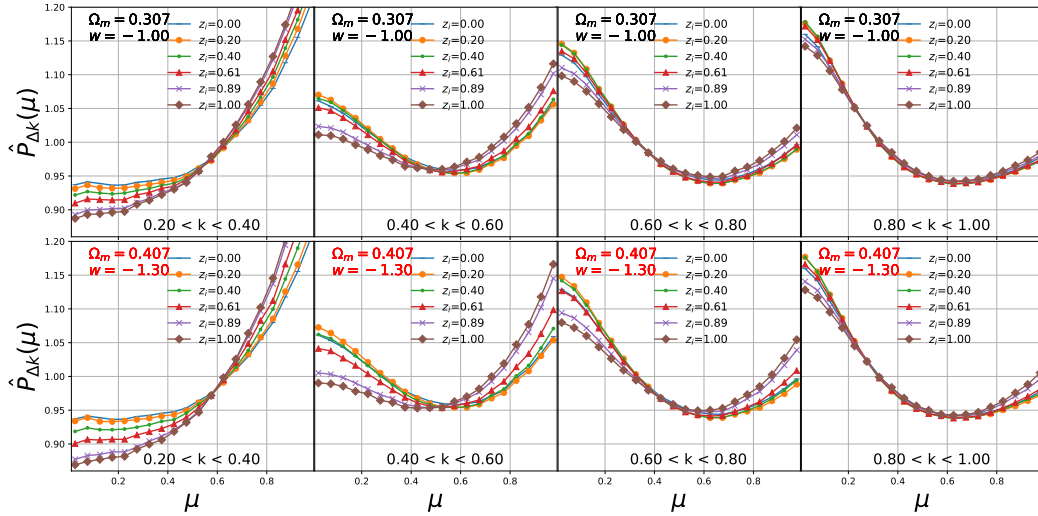


FIG. 3.— The integrated 2D PS $\hat{P}_{\Delta k}(\mu)$ measured at 6 redshifts, in the underlying true cosmology (upper panels) and a wrong cosmology ($\Omega_m = 0.407, w = -1.3$) (text marked in red), respectively. In both cases we detect large anisotropy mainly produced by the RSD effect. In the wrong cosmology case, a larger redshift evolution of $\hat{P}_{\Delta k}(\mu)$ produced by the AP distortion is detected.

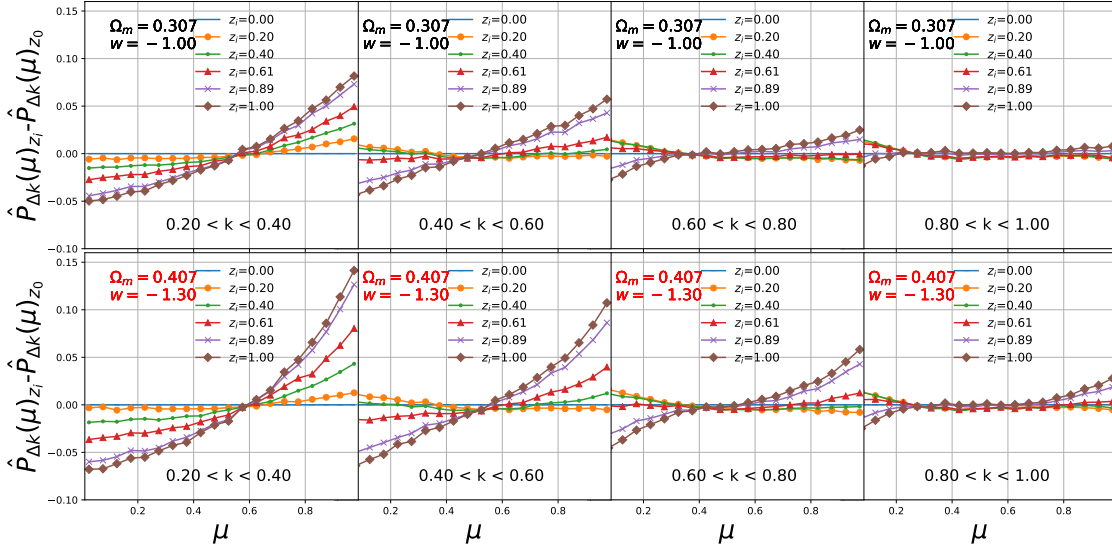


FIG. 4.— The redshift evolution of $\hat{P}_{\Delta k}(\mu)$ between redshifts z_i and z_0 , where we chose $z_0 = 0$ and $z_i = 0.2, 0.4, 0.61, 0.89, 1.0$. A larger redshift evolution is detected in the wrong cosmology. The integration range of k is chosen as $(0.2, 0.4)$, $(0.4, 0.6)$, $(0.6, 0.8)$ and $(0.8, 1)$ $h \text{ Mpc}^{-1}$, respectively.

TABLE 1
 $\delta \hat{P}_{\Delta k}(\mu = 1, z_1 = 0, z_2 = 1)$ IN THE TRUE COSMOLOGY AND A WRONG COSMOLOGY $\Omega_m = 0.407, w = -1.30$

Integration range of k ($h \text{ Mpc}^{-1}$)	(0.2, 0.4)	(0.4, 0.6)	(0.6, 0.8)	(0.8, 1.0)	(0.2, 0.6)	(0.6, 1.0)	(1.4, 1.8)
$\delta \hat{P}_{\Delta k, \text{true cosmology}}$	8.16×10^{-2}	5.73×10^{-2}	2.49×10^{-2}	7.86×10^{-3}	7.35×10^{-2}	1.74×10^{-2}	1.83×10^{-3}
$\delta \hat{P}_{\Delta k, \text{wrong cosmology}}$	1.41×10^{-1}	1.07×10^{-1}	5.82×10^{-2}	2.79×10^{-2}	1.30×10^{-1}	4.48×10^{-2}	3.98×10^{-3}
$\delta \hat{P}_{\Delta k, \text{wrong cosmology}} / \delta \hat{P}_{\Delta k, \text{true cosmology}}$	1.73	1.87	2.34	3.55	1.77	2.58	2.17

Since now, we are measuring the PS from samples that have a constant number density $\bar{n} = 10^{-3} (h^{-1} \text{Mpc})^{-3}$. To test the effect of *selection bias*, it is necessary to test the results from samples having different number density.

In Fig. 7, we plot the integrated PS $P_{\Delta k}(\mu)$ in 7 subsamples of the $z = 0$ halos lying in different mass ranges, including $(0.2, 0.4)$, $(0.4, 0.6)$, $(0.6, 0.8)$, $(0.8, 1.0)$, $(1.0, 2.0)$, $(2.0, 5.0)$ and $(5.0, 10.0)$ in units of $10^{13} M_{\odot}$. We use $k \in (0.2, 1.8) h \text{ Mpc}^{-1}$ in all curves.

Clearly, the clustering strength varies significantly among the subsamples, resulting in 10% – 1500% difference among their $P_{\Delta k}(\mu)$ s (left panel). In contrast, after the amplitude normalized, the $\hat{P}_{\Delta k}(\mu)$ s from the difference subsamples are rather similar. The largest discrepancy appears in the subsample with a mass range $(0.2, 0.4) \times 10^{13} M_{\odot}$, whose results have a 5% difference from the others. For the other subsamples, the difference among their $\hat{P}_{\Delta k}$ is $\lesssim 2\%$.

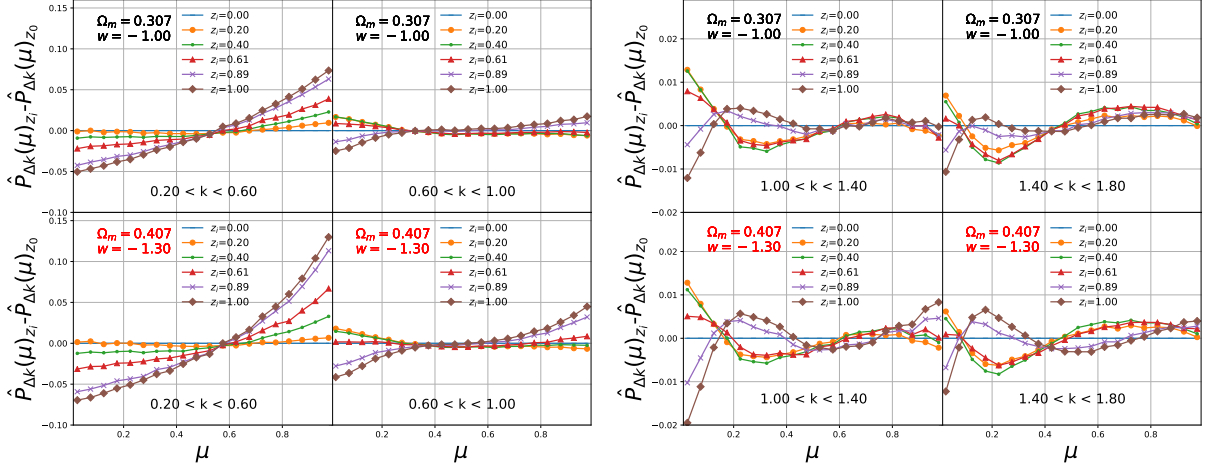


FIG. 5.— The redshift evolution of $\hat{P}_{\Delta k}(\mu)$ in cases that the range of k chosen as (0.2,0.6), (0.6,1), (1,1.4) and (1.4,1.8) in units of $h \text{ Mpc}^{-1}$, respectively. The tomographic AP method works well throughout the regime of k .

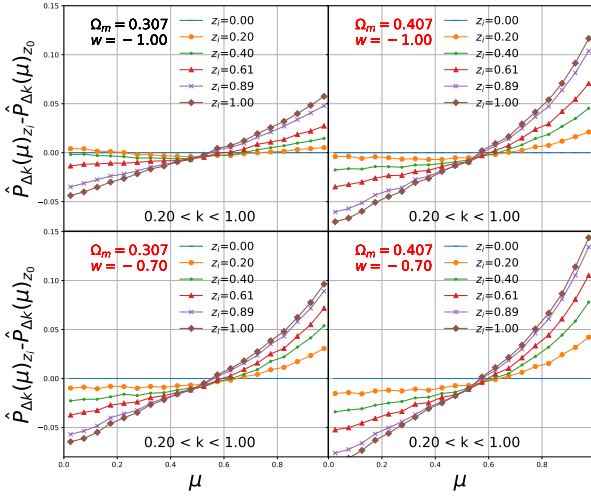


FIG. 6.— The redshift evolution of $\hat{P}_{\Delta k}(\mu)$ measured in the underlying true cosmology and three wrong cosmologies. We find significantly larger evolution in all wrong cosmologies.

5. CONCLUSIONS AND DISCUSSIONS

In this work, we study the feasibility of conducting the tomographic AP test using the PS statistics. Similar to Li et al. (2015), we quantify the anisotropic clustering by $\hat{P}_{\Delta k}(\mu)$, and use its redshift evolution $\delta\hat{P}_{\Delta k}$ to probe the AP effect. To test the method, we use dark matter halos from the BigMD simulation, and created from it a set of constant number density samples having $\bar{n} = 10^{-3}(h^{-1}\text{Mpc})^{-3}$ at redshifts of 0.2, 0.4, 0.61, 0.89 and 1.0. The “true” cosmology (i.e. the simulation cosmology) has cosmological parameters of $\Omega_m = 0.3071, w = -1$.

In the incorrect cosmologies of $(\Omega_m, w) = (0.407, -1), (0.307, -0.7)$ and $(0.407, -0.7)$, we measured larger values of $\delta\hat{P}_{\Delta k}$ than in the true cosmology. This means that the AP effect manifests itself as a redshift-dependent anisotropy in the clustering of structures, and is successfully captured by the PS analysis. Adjusting the integration interval of k in ranges of 0.2-1.8 $h \text{ Mpc}^{-1}$, we find that the $\delta\hat{P}_{\Delta k}$ in the cosmology $\Omega_m = 0.407, w = -1.3$ was enlarged by a factor of approximately 1.7-3.6.

We emphasize that the clustering scales explored in this work and the previous works Li et al. (2014, 2015, 2016) are quasi- or highly non-linear. Accurate modeling of $\xi(s, \mu)$ or $P(k, \mu)$ in this region is of great difficulty. Our method provides a way to extract cosmological information in this region without having their accurate theoretical predictions.

By focusing on much smaller scales the information explored by the tomographic AP method is intrinsically different and largely independent from those explored by traditional methods such as BAO (which mainly use $k \lesssim 0.1 h \text{ Mpc}^{-1}$). A simple check performed in (Zhang et al. 2019) showed that the correlation between the two methods is close to zero.

We explore the non-linear clustering scale up to $k = 1.8 h \text{ Mpc}^{-1}$, and find that the tomographic AP method still work well in that regime. This is tremendously difficult for most current methods. On smaller scales, the effect of baryons may become important, and it is not enough to study it just using pure dark matter simulation.

In Fourier space we may have advantages of mode-decoupling, easier theoretical prediction, clearer physical meaning, and sometimes faster computational speed. But we can not claim that it is a better choice than the configuration space just based on these arguments. An advantage of using the configuration space is that, the FOG effect is constrained in the $\lesssim 10 h^{-1} \text{ Mpc}$ (in PS, after a Fourier transform the FOG effect spreads out within a large (k, μ) range), so it is easy to control it. In any case, it is helpful to have the results derived in both Fourier and configuration spaces, which are cross-checks of each other.

In this proof-of-concept work we have not predicted the power of the method in constraining Ω_m and w , which requires calculating the covariance matrix of $\delta\hat{P}_{\Delta k}(\mu)$ using a large number of realizations. We leave this for future for when we apply the method to real observational data.

We thank Gong-bo Zhao and Yuting Wang for very helpful suggestions. XDL acknowledges the supported from NSFC grant (No. 11803094). CGS acknowledges financial support from the National Research Foundation of Korea (NRF; #2017R1D1A1B03034900, #2017R1A2B2004644 and #2017R1A4A1015178).

ZL was supported by the Project for New faculty of Shang-

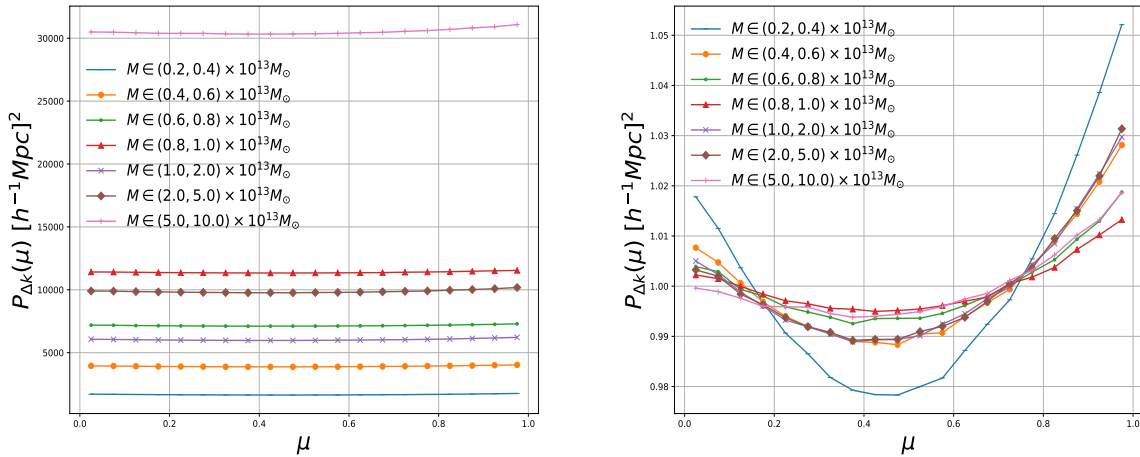


FIG. 7.— The influence of halo bias on the statistical quantity $P_{\Delta k}(\mu)$. When changing the mass of halos in range of $2 \times 10^{12} - 10^{14} M_{\odot}$, we detect significant change in the clustering strength (left panel). After the normalization, $\hat{P}_{\Delta k}(\mu)$ becomes rather insensitive to the halo mass.

hai JiaoTong University (AF0720053), the National Science Foundation of China (No. 11533006, 11433001) and the National Basic Research Program of China (973 Program 2015CB857000).

The CosmoSim database used in this paper is a service by the Leibniz-Institute for Astrophysics Potsdam (AIP). The MultiDark database was developed in cooperation with the Spanish MultiDark Consolider Project CSD2009-00064.

REFERENCES

- Alam, S., Ata, M., Bailey, S., et al. 2017, MNRAS, 470, 2617
 Alcock, C., & Paczynski, B. 1979, Nature, 281, 358
 Anderson, L., Aubourg, E., Bailey, S., et al. 2012, MNRAS, 427, 3435
 Ballinger, W. E., Peacock, J. A., & Heavens, A. F. 1996, MNRAS, 282, 877
 Behroozi, P. S., Wechsler, R. H., & Wu, H.-Y. 2013, ApJ, 762, 109
 Beutler, F., Blake, C., Colless, M., et al. 2012, MNRAS, 423, 3430
 Bianchi, D., Gil-Marín, H., Ruggeri, R., & Percival, W. J. 2015, Mon. Not. Roy. Astron. Soc., 453, L11
 Blake, C., Glazebrook, K., Davis, T. M., et al. 2011a, MNRAS, 418, 1725
 Blake, C., Brough, S., Colless, M., et al. 2011b, MNRAS, 415, 2876
 Colless, M., Peterson, B. A., Jackson, C., et al. 2003, arXiv Astrophysics e-prints, astro-ph/0306581
 Eisenstein, D. J., Zehavi, I., Hogg, D. W., et al. 2005, ApJ, 633, 560
 Hand, N., Feng, Y., Beutler, F., et al. 2018, Astron. J., 156, 160
 Kaiser, N. 1987, MNRAS, 227, 1
 Kim, J., Park, C., Gott III, J. R., & Dubinski, J. 2009, The Astrophysical Journal, 701, 1547
 Kim, J., Park, C., L'Huillier, B., & Hong, S. E. 2015, arXiv preprint arXiv:1508.05107
 Klypin, A., Yepes, G., Gottlöber, S., Prada, F., & Heß, S. 2016, MNRAS, 457, 4340
 Lavaux, G., & Wandelt, B. D. 2012, ApJ, 754, 109
 Li, M., Li, X.-D., Wang, S., & Wang, Y. 2011, Communications in Theoretical Physics, 56, 525
 Li, X.-D., Miao, H., Wang, X., et al. 2019, ApJ, 875, 92
 Li, X.-D., Park, C., Forero-Romero, J. E., & Kim, J. 2014, Astrophys. J., 796, 137
 Li, X.-D., Park, C., Sabiu, C. G., & Kim, J. 2015, Mon. Not. Roy. Astron. Soc., 450, 807
 Li, X.-D., Park, C., Sabiu, C. G., et al. 2016, Astrophys. J., 832, 103
 Li, X.-D., Sabiu, C. G., Park, C., et al. 2018, Astrophys. J., 856, 88
 Mao, Q., Berlind, A. A., Scherrer, R. J., et al. 2017, ApJ, 835, 160
 Matsubara, T., & Suto, Y. 1996, ApJ, 470, L1
 Outram, P. J., Shanks, T., Boyle, B. J., et al. 2004, MNRAS, 348, 745
 Park, H., Park, C., Sabiu, C. G., et al. 2019, arXiv:1904.05503
 Percival, W. J., Cole, S., Eisenstein, D. J., et al. 2007, MNRAS, 381, 1053
 Perlmutter, S., Aldering, G., Goldhaber, G., et al. 1999, ApJ, 517, 565
 Ramanah, D. K., Lavaux, G., Jasche, J., & Wandelt, B. D. 2019, A&A, 621, A69
 Riess, A. G., Filippenko, A. V., Challis, P., et al. 1998, AJ, 116, 1009
 Ryden, B. S. 1995, ApJ, 452, 25
 Scoccimarro, R. 2015, Phys. Rev., D92, 083532
 Wang, Y. 2008, Phys. Rev., D77, 123525
 Weinberg, D. H., Mortonson, M. J., Eisenstein, D. J., et al. 2013, Phys. Rep., 530, 87
 Weinberg, S. 1989, Reviews of Modern Physics, 61, 1
 York, D. G., Adelman, J., Anderson, Jr., J. E., et al. 2000, AJ, 120, 1579
 Zhang, Z., Gu, G., Wang, X., et al. 2019, Astrophys. J., 878, 137
 Zheng, Y., & Song, Y.-S. 2016, JCAP, 1608, 050